SUPPORTING INFORMATION

Strain stiffening and compression-induced softening of composite fibrous hydrogels derived from rod-shaped nanoparticles and a synthetic copolymer

Sofia Morozova,[a,b] *Yingshan Ma*[a] *Vahid Adibnia,*[c] *Eugenia Kumacheva**[a,d,e]

a. Department of Chemistry, University of Toronto, Toronto, ON, M5S 3H6, Canada,
b. Moscow Center for Advanced Studies, Kulakova Str. 20, 123592 Moscow, Russia,
c. Department of Chemistry, Dalhousie University, Halifax, NS B3H 4R2, Canada
d. Department of Chemical Engineering and Applied Chemistry, University of Toronto, Toronto, ON, M5S 3E5, Canada
e. The Institute of Biomedical Engineering, University of Toronto, Toronto, ON, M5S 3G9, Canada

Correspondence to: eugenia.kumacheva@utoronto.ca (Prof. Eugenia Kumacheva), sofiiionova@ya.ru (Dr. Sofia Morozova)

Keywords: fibrillar gel, cellulose nanocrystals, nonlinear mechanics, nanocolloidal gel, strain-stiffening

S1. Hydrogel preparation

S1.1. Synthesis and characterization of the copolymers

The copolymer was synthesized by free-radical copolymerization of acrylamide (Am) and acrylic acid hydrazide (Hyd). Acrylic acid hydrazide protected with tert-butoxycarbonyl group (Hyd-Boc) was deprotected by the reaction with 1M HCl(aq), as previously described[1–3] (**Fig. S1a**).

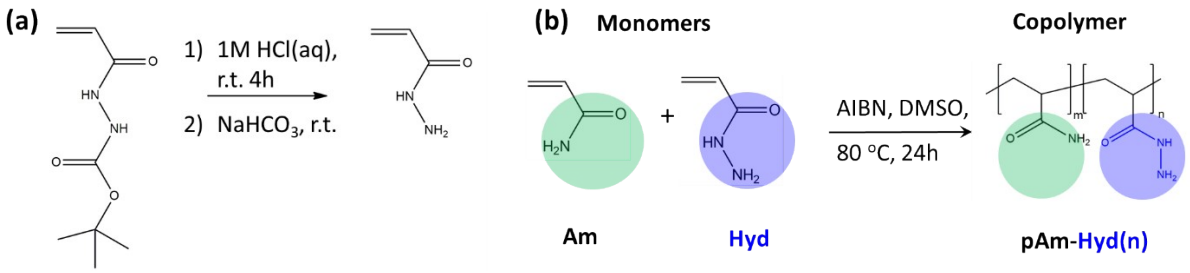

Fig. S1. Synthesis and characterization of copolymers. (a) Scheme of deprotection of acryloyl hydrazide. (b) Scheme of synthesis of pAm-Hyd(2), pAm-Hyd(5), pAm-Hyd(9) and pAm-Hyd(23) copolymers.

A solution of Hyd-Boc (3.0 g, 16.1 mmol) in 1 M $HCl_{(aq)}$ (100 mL) was stirred at room temperature for 4 h. Then, a 0.1M $NaHCO_3$ solution was added dropwise until pH=7.0 was reached. The reaction mixture was extracted with diethyl ether (Et_2O, 30 mL, 5 times), and the combined extract was dried under reduced pressure without heating to obtain white crystalline powder (1.1 g, 50% yield): ^{1}H-NMR (300 MHz, D_2O), δ (ppm): 8.45 (s, 1H), 6.21-6.44 (m, 2H), 5.72 (m, 1H). The extracted monomer was immediately used in free-radical copolymerization with Am monomer to obtain copolymers with a varying molar concentration of the Hyd comonomer, c_{Hyd} (**Fig. S1b**). The copolymers denoted as pAm-Hyd(2), pAm-Hyd(5), pAm-Hyd(9) and pAm-Hyd(23) (main text) contained 2.0, 4.8, 9.1 and 23.1 mol.% of the Hyd comonomer, respectively. The recipes for the copolymer synthesis are provided in **Table S1**.

The comonomers were dissolved in 40 mL of anhydrous dimethyl sulfoxide (DMSO) in a two-neck round bottom flask equipped with septa and purged with nitrogen. Then initiator, AIBN, were dissolved in 1 mL of DMSO and added using syringe through septa to the solution of comonomers. The flask with the solution was placed to an oil bath at 80 °C and polymerization reaction was performed for 24 h at 80 °C under nitrogen atmosphere. Then, the reaction mixture was cooled down to r.t. and DMSO (10 mL) was added to the reaction mixture to decrease its viscosity. The polymer was precipitated in excess of diethyl ether and dried at r.t. and under vacuum. The copolymer was obtained at 84-92% yield and stored as white powder at 5-10°C.

Table S1. Recipes for copolymer synthesis

Notation	c_{Hyd}, wt. %[a)]	Am, g	Hyd, g	AIBN, g
pAm-Hyd(2)	2.0	3.900	0.095	0.0083
pAm-Hyd(5)	4.8	3.750	0.227	0.0083
pAm-Hyd(9)	9.1	3.560	0.431	0.0083
pAm-Hyd(23)	23.1	2.900	1.054	0.0080

The molecular weight of the copolymers was studied by gel-permeation chromatography (GPC) in 0.1M LiBr in dimethyl formamide (DMF) using poly(methyl methacrylate) standards. The GPC traces are shown in **Fig. S2**. copolymers.

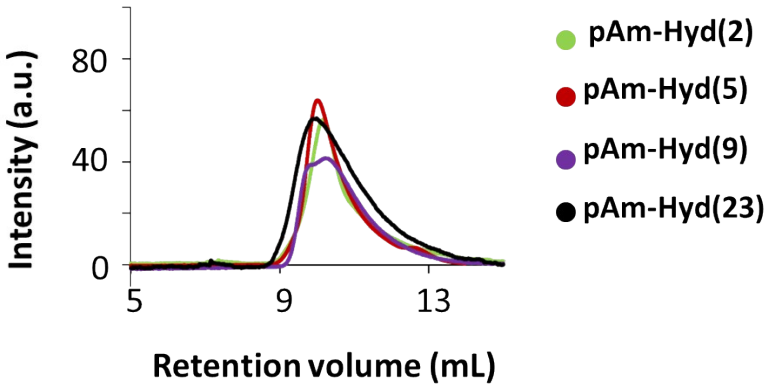

Fig. S2. Copolymer characterization. Gel permeation chromatography (GPC) traces of the copolymers. in 0.1M LiBr in dimethylformamide.

The copolymers had the molecular weight in the range of 40 000 – 55 000 Da and polydispersity index (PDI) of 1.51-1.72 (**Table S2**).

Table S2. Characteristics of the copolymers

Notation	c_{Hyd}, %[a]	cNH-NH$_2$ (theor.) [mmol/g][b]	cNH-NH$_2$ (exp.) [mmol/g][c]	M_n[d]	PDI [d]	T_g, °C[e]
pAm-Hyd(2)	2.0	0.28	0.29±0.04	55 000	1.51	165
pAm-Hyd(5)	4.8	0.70	0.70±0.15	45 000	1.63	160
pAm-Hyd(9)	9.1	1.38	1.35±0.190	40 000	1.55	170
pAm-Hyd(23)	23.1	3.97	3.66±0.720	45 000	1.72	190

[a] Molar concentrtaion of Hyd monomer during synthesis; [b] Theoretical concentration of NH-NH_2 groups in the copolymer; [c] Experimentally determined concentration of NH-NH_2 groups in the copolymer by TNBS assay; [d] Determined by GPC; [e] Determined by differential scanning calorimetry.

The presence of the hydrazide groups in the copolymers was confirmed by the 2,4,6-trinitrobenzenesulfonic acid (TNBS) assay, as reported elsewhere.[4] The hydrazide groups reacted with TNBS to form a colored derivative compound (**Fig. S3a**) which was quantitatively identified by ultraviolet-visible (UV-Vis) spectroscopy using tert-butyl carbazate (TBZ)-based calibration curve (**Fig. S3b**). The concentration of the hydrazide groups in the copolymers, c_{NH2}, was 0.29, 0.70, 1.35 and to 3.66 mmol/g for pAm-Hyd(2), pAm-Hyd(5), pAm-Hyd(9) and pAm-Hyd(23), respectively.

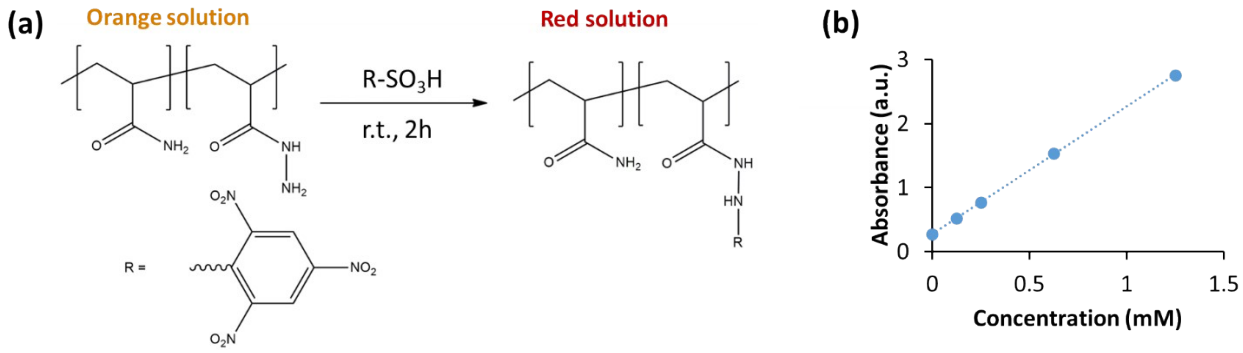

Fig. S3. Characterization of the copolymer. (a) Reaction scheme of the 2,4,6-trinitrobenzenesulfonic acid (TNBS) assay for determination of hydrazide groups in the copolymer. (b) Calibration graph of TBZ in the TNBS assay used for the determination of the concentration of the hydrazide groups in the copolymer.

A random, rather than blocky distribution of the monomer units in the copolymer, was expected from the similarity of the reaction constants[5,6] and validated by measuring a single glass transition temperature (T_g) of the copolymers (**Table S2**). The increase in T_g with an increasing fraction of hydrazide groups in the copolymer was attributed by the formation of hydrogen bonds and cyclic structures between amide and hydrazide groups.[7]

S1.2. Functionalization of CNCs with aldehyde groups

Aldehyde-modified cellulose nanocrystals (aCNCs) were prepared by oxidizing hydroxyl groups pristine CNCs using sodium periodate **(Fig. S4a).** Possible CNC damage during their oxidation with sodium periodate[8,9] was examined using transmission electron microscopy (TEM). **Fig. S4b** and **b′** show TEM images of pristine and aldehyde-modified CNCs. Analysis of the TEM images using ImageJ program (National Institute of Health, USA) revealed that after

oxidation, the average CNC length decreased from 160±45 to 145±35 nm (**Fig. S4c**), while the average diameter was 15±5 nm (**Fig. S4d**). The CNC length change can be considered insignificant and the high aspect ratio of aCNCs was sufficient for the formation of fibrous gels.

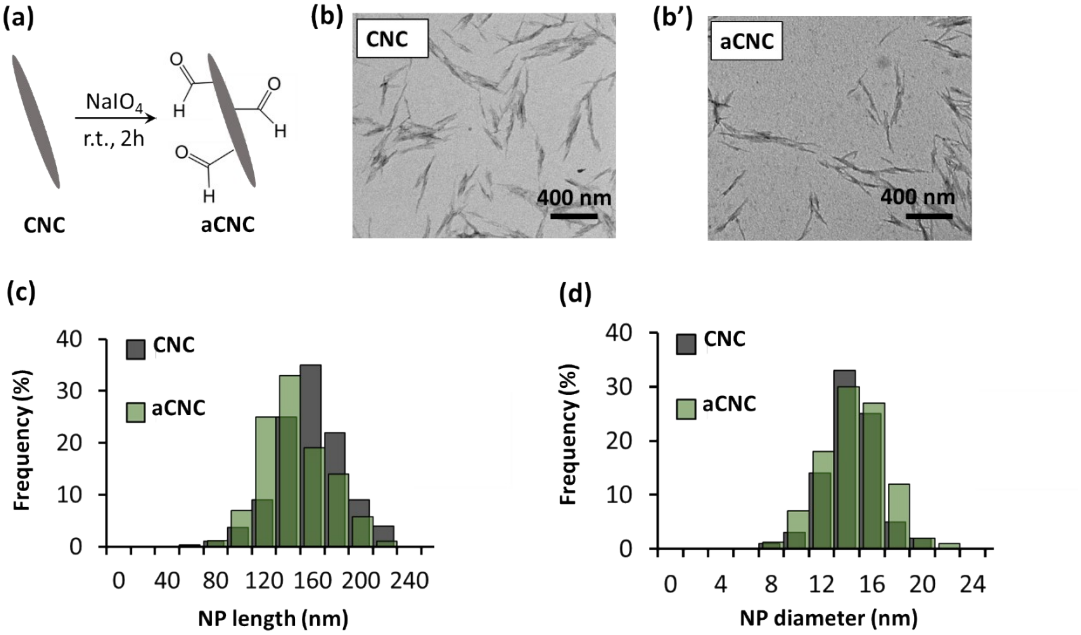

Fig. S4. Characterization of aldehyde-modified aCNCs; (a) Scheme of surface modification of aCNCs; (b-b′) Transmission electron microscopy images of pristine CNCs (b) and aCNCs (b′); (c-d) Histograms of the length (c) and diameter (d) of pristine CNCs (CNC) and aCNCs, n=100;

The concentration of aldehyde groups on the aCNCs was determined by reacting aCNCs with TBZ for hydrazone bond formation and subsequently, determining the amount of unreacted TBZ using the TNBS assay and the TBZ calibration curve (**Fig. S3b**) as described elsewhere.[10] The concentration of aldehyde groups on aCNC was 3.88 mmol/g, in agreement with previously reported data[8,9] and almost equimolar with the concentration of hydrazide groups in pAm-Hyd(23).

S1.3 Hydrogel preparation

The hydrogel was prepared by mixing an aqueous aCNC suspension in Hanks′ Balanced Salt solution (1xHBSS)[11] and a copolymer aqueous solution to form hydrazone covalent crosslinks between the aldehyde groups of aCNCs and the hydrazide groups of the copolymer. The concentration of hydrazone crosslinks, $c_{\text{hydrazone}}$, in the hydrogels was characterized by determining the concentration of unreacted aldehyde groups on the aCNC surface using TBZ and a TNBS assays (**Fig. S5**).

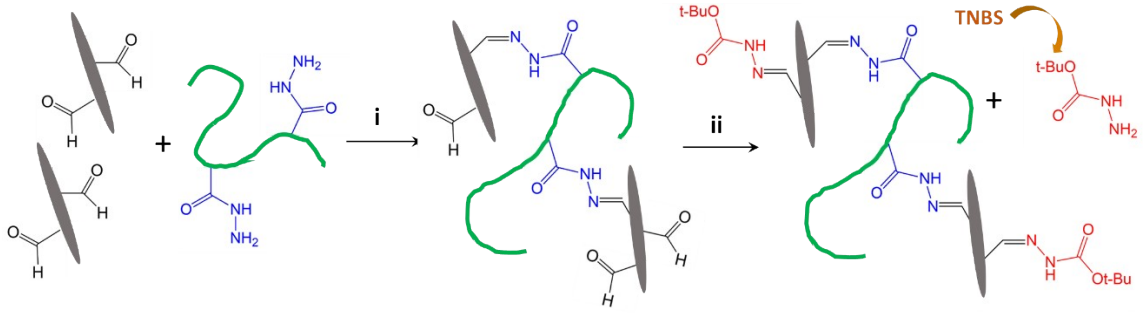

Fig. S5. Hydrogel formation and characterization of the concentration of hydrazone crosslinks in the hydrogel. Scheme of the reaction leading to hydrogel formation and TNBS assay. (i) Formation of hydrazone crosslinks between aCNCs and hydrazide groups of the copolymer (marked with blue color). (ii) Formation of hydrazone crosslinks between aCNCs and TBZ (red), with unreacted TBZ determined by TNBS assay;

S2. Characterization of the hydrogel structure

S2.1. Scanning electron microscopy

The structure of the hydrogels was examined by scanning electron microscopy (SEM). The samples for imaging were prepared by using supercritical CO_2 drying.[12] **Fig. S6** shows representative SEM images of the structure of hydrogels Gel-H2, Gel-H5, Gel-H9 and Gel-H23, respectively.

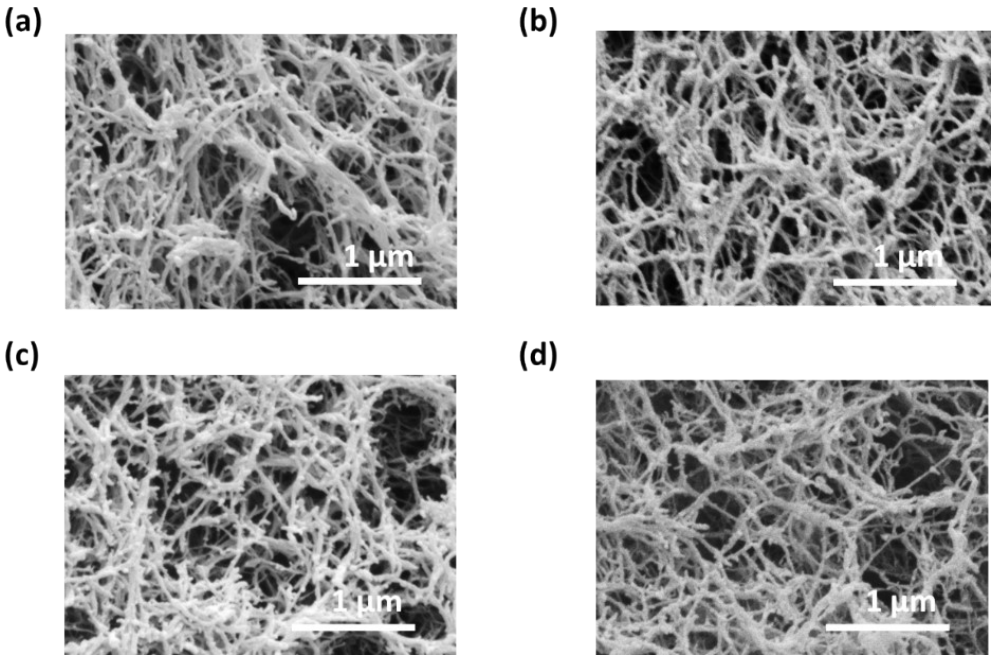

Fig. S6. Representative SEM images of Gel-H2 (a), Gel-H5 (b), Gel-H9 (c) and Gel-H23 (d). All hydrogels were formed at the copolymer/aCNC mass ratio 1/1 and c_{tot}=3.0 wt%.

All hydrogels had a fibrillar structure that was typical for composite CNC-derived hydrogels.[11,13,14]

S2.2 Measurement of Darcy permeability of the hydrogels

Darcy permeability of the hydrogels was determined using a pressure-driven flow model in poly(dimethyl siloxane) (PDMS) microfluidic device.[15] The Darcy permeability coefficient, K_s, was determined as[16]

$$K_s = \frac{\eta L_{gel} Q_p}{A \Delta P}, \quad \text{(S1)}$$

where η is the viscosity of water (1.002 cP at 22 °C[17]), L_{gel} is the hydrogel length; Q_p is the volumetric flow rate, of water through the hydrogel, ΔP is the pressure difference across the hydrogel, and A is the cross-sectional area of the hydrogel. The linear dependence of Q_p *vs.* ΔP in the range of applied pressures indicated that the hydrogel structure was not affected by the pressure-driven flow (**Fig. S7**).

The average pore size, ξ, was calculated as [16]

$$\xi = 2\sqrt{\frac{8K_s}{1-\varphi}}, \quad \text{(S2)}$$

where φ is the volume fraction of the fibers in the gel.

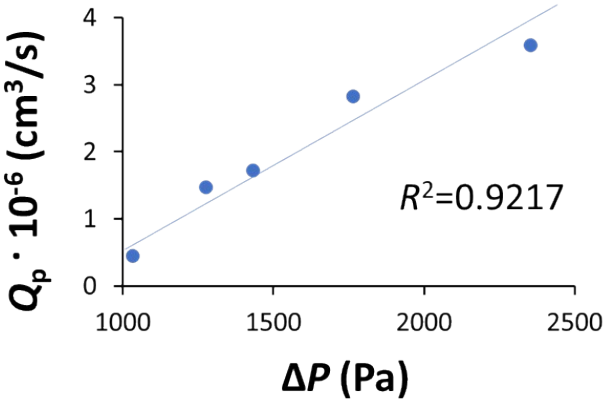

Figure S7. Measurement of Darcy permeability of hydrogels. Dependence of the volumetric flow rate, Q_p, on the applied pressure difference, ΔP, for hydrogel.

S2.3 Characterization of hydrogel swelling

The degree of swelling of the hydrogels in water was studied by measuring the equilibrium mass change of the hydrogels subjected to supercritical drying. The degree of swelling, α_S, was determined as $\alpha_S = [(m_t - m_0)/m_0] \times 100\%$, where m_0 is the mass of the dried hydrogel and m_t is the mass of hydrogel at a particular time of its swelling in water.

The change in mass was measured by weighing the samples over a period of 5 h. Fig. S8 shows that the degree of swelling of the hydrogels in aqueous media determined a was from 34 to

21% when the concentration of crosslinking groups, $c_{hydrazone}$, changed from 280±67 to 3570±750 μmol/g, respectively.

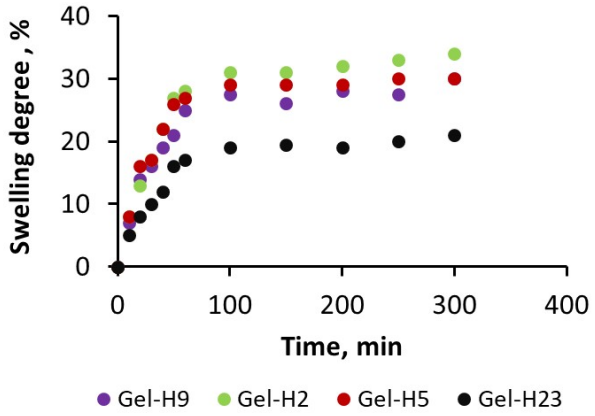

Fig. S8. Variation in the degree of swelling of Gel-H2 , Gel-H5, Gel-H9 and Gel-H23. All hydrogels were formed at the copolymer/aCNC mass ratio 1/1 and c_{tot}=3.0 wt%.

S3. Characterization of the structure and mechanical properties of filaments

Our group has shown that nonlinear mechanical properties of athermal enthalpic fibrous networks are described by the affine model.[14,16] In this model, the constituent fibers of the gel are characterized by their stretching modulus, k_S, and bending modulus, k_b. By analyzing SEM images of the hydrogels, we calculated the apparent geometric characteristics of the filaments (that is, the fiber fragments between two crosslinking points), namely, the contour length, L_0, the end-to-end distance of the filament, R_0, and filament diameter, d_f., as illustrated in **Fig. S9**.

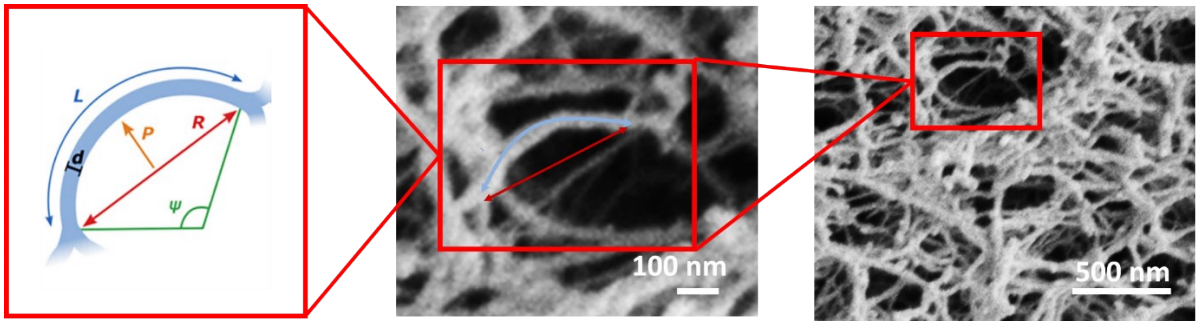

Fig. S9. Analysis of filament characteristics in the hydrogel. *Left*: A scheme of an individual filament with contour length, L_0, end-to-end distance, R_0, diameter, d_f, deflection, P_0, and arc angle, ψ. *Middle*: Enlarged exemplary SEM image of the analyzed characteristics of the filament. The red solid line shows the end-to-end distance of the filament and the blue line shows its to contour length. *Right*: Exemplary SEM image of the hydrogel.

Although the SEM imaging was performed for the samples prepared by the CO2 supercritical drying method, we admit that filament geometric characteristics obtained by

analyzing SEM images may not exactly represent the corresponding dimensions in the swollen gel state and are therefore called “apparent” in main text. Analysis of SEM images of the hydrogels yielded the projection of the filament’s apparent contour length, l, projection of the apparent end-to-end distance, r, and fiber diameter, d_f. We then calculated the projection, p, of the apparent distance between filament center and the center of end-to-end distance (hence, deflection) as

$$p = \frac{1}{4}\sqrt{6l(l-r)} \tag{S3}$$

Table S3 shows the analyzed structural apparent characteristics of the filaments in the hydrogels .

Table S3. Structural apparent characteristics of filaments in the hydrogels

Gel	***r, nm***	***p, nm***	***l*, nm**
Gel-H2	380	104	445
Gel-H5	368	92	422
Gel-H9	366	87	415
Gel-H23	362	84	408

To link the 2D projected characteristics of the filaments and their theoretically apparent values we used characteristics, the following equations were used[14]

$$R_0 = \sqrt{\frac{3r^2}{2}} \tag{S4}$$

$$P_0 = \sqrt{\frac{p^2}{r^2(r^{-2} - 0.5pR_0^{-2})}} \tag{S5}$$

Next, we calculated the apparent end-to-end distance, L_0, between the crosslinking points in the hydrogels and an apparent arc angle, ψ_0 of the filament as [14]

$$\Psi_0 = 4arctan(\frac{2P_0}{R_0}) \tag{S4}$$

$$L_0 = \frac{24R_0}{24 - \Psi_0^2} \tag{S5}$$

Based on the experimentally measured storage shear modulus, G', of the gel and its average pore size, ξ (determined by measuring Darcy permeability of the hydrogel) we calculated the mechanical modulus E of the gel as [14]

$$E = \frac{4\xi^2 \Psi_0^2 L_0^2 G'}{9\pi d_f^2} \quad \text{(S6)}$$

Next, we calculated the apparent persistence length, l_p of the filaments

$$l_p = \frac{E d_f^4}{kT} = \frac{4\xi^2 \Psi_0^2 L_0^2 G' d_f^2}{9\pi kT} \quad \text{(S7)}$$

Finally, we determined the filament apparent stretching modulus, k_S, the apparent bending modulus, k_b, and apparent Ψ_c (the critical angle at which the filaments bend more than stretch) as

$$k_s = \frac{\pi E d_f^2 L_0}{4} = \frac{\xi^2 \Psi_0^2 L_0^3 G'}{9 d_f^2} \quad \text{(S8)}$$

$$L_0 = \frac{9\pi E d_f^4}{4 d \Psi_0^2 L_0} = \xi^2 L_0 G \quad \text{(S9)}$$

$$\Psi_c = \sqrt{\frac{L_0}{l_p}} \quad \text{(S10)}$$

$$k_b = \frac{9\pi E d_0^4}{4\psi_0^2 L} = \xi^2 L_0 G \quad \text{(S11)}$$

Based on Eqs. 4-10, we calculated the apparent deflection, P_0, apparent persistence length, l_p, apparent arc angle, Ψ_0, and Ψ_c of the filaments (Table S4)

Table S4. Structural apparent characteristics of hydrogels

Gel	d_f, nm[a]	R_0, *nm*	P_0, *nm*	L_0, nm	l_p, μm	Ψ_0	Ψ_c
Gel-H2	29 ± 7	465± 25	128	559± 40	715	2.00	0.06
Gel-H5	29 ± 6	450± 25	113	529± 60	3 036	1.86	0.06
Gel-H9	29 ± 5	448± 25	107	517± 60	7 536	1.78	0.06
Gel-H23	29 ± 8	443± 30	103	507± 60	36 637	1.73	0.06

[a] Determined by analyzing SEM images

In all hydrogels the filaments had a similar end-to-end distance, ranging from 465 to 443 nm and an identical fiber diameter, d_f, of 29±7 nm. The contour lengths of the filaments in all hydrogels were similar, while the softest Gel-H2 contained approximately 20% longer filaments. Yet, due to the difference in mechanical properties of the fibers, the apparent persistence length, l_p, of the filaments in the hydrogels was different. For example, it was 715 and 36 637 μm in the softest and the stiffest gels, respectively.

Table S5 shows the apparent bending modulus, k_b, and apparent stretching modulus, k_S, and their ratios for the filaments in the hydrogels with a different degree of intrafibrillar crosslinking. The filaments in Gel-H2, Gel-H5, Gel-H9, and Gel-H23 had $k_s\ k_b \gg 1$.

Table S5. Mechanical properties of hydrogel filaments

Gel	k_b $*10^{-15}$(J)	k_s $*$ $_{10^{-15}}$ (J)	k_s/k_b
Gel-H2	0.010	1.59	166
Gel-H5	0.050	6.39	128
Gel-H9	0.139	15.6	112
Gel-H23	0.725	74.7	103
EKGel[a]	0.050	5.73	115

[a] The data are taken from ref.[14] for the hydrogel prepared from aCNCs and gelatin with gelatin/aCNC mass ratio 1/1 and c_{tot}=3.0 wt%.;

Figure S10a shows the frequency sweeps for the hydrogels in the frequency range of 0.1-3.0 Hz at strain amplitude of 1%. For all gel compositions, the ratio G''/G' was below 1.0 in the plateau (elastic) region.

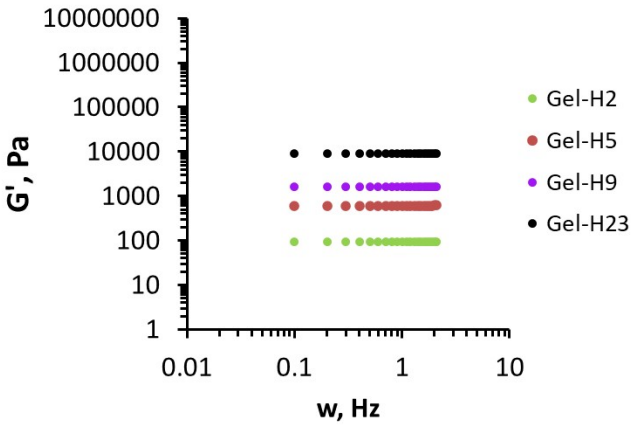

Fig. S10. Variation in shear storage modulus G' with frequency for gels with different compositions. The experiments were conducted at strain of 1% and the temperature of 22°C.

Figure S11 shows representative stress–strain curves used to extract Young's modulus of the hydrogels. The compression Young's modulus was calculated from the slope of the linear region corresponding to 10% of deformation on stress-strain curves.

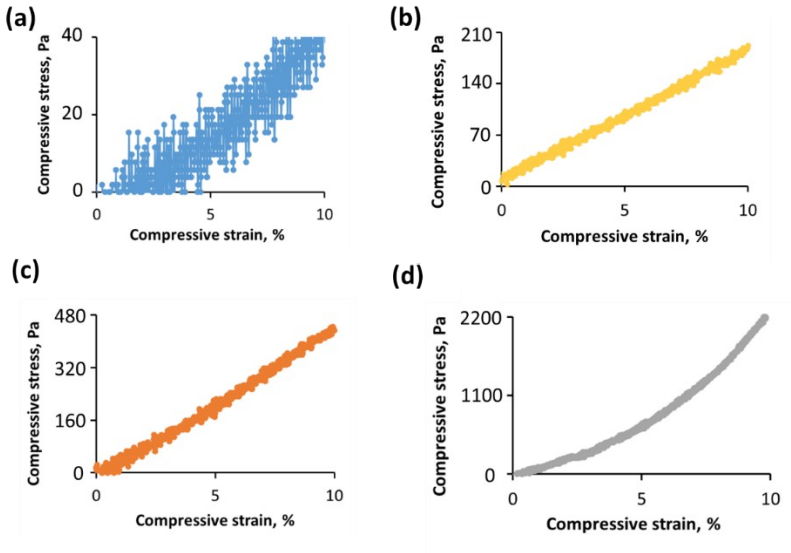

Fig. S11. Representative stress–strain curves in compression experiments used to extract Young's modulus of (a) Gel-H2, (b) Gel-H5, (c) Gel-H9 and (d) Gel-H23. The strain rate was 0.01 s^{-1}.

The mechanical properties of the hydrogels were studied at 22 °C and biologically relevant temperature of 37 °C. **Figure S12a** and **b** show the variation in the hydrogel shear storage modulus, *G*', and loss modulus, *G*", determined in the oscillation rheology experiments at 1% strain and 1 Hz frequency.

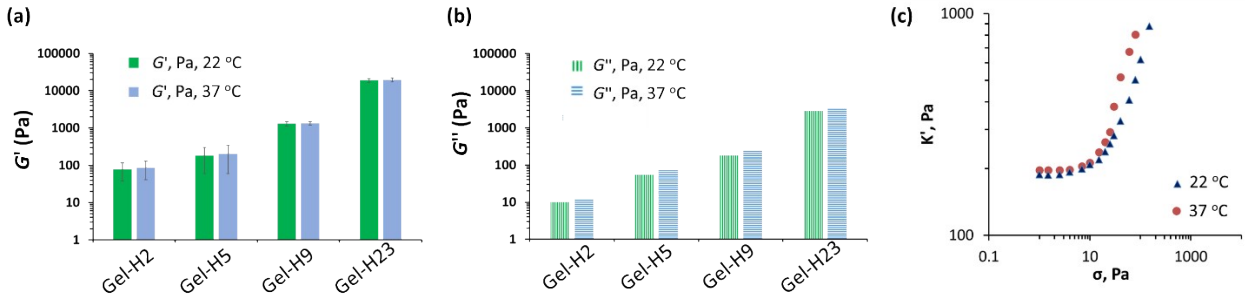

Fig. S12. Mechanical properties of the hydrogels. Variation in the storage modulus, *G*' (a) and *G*" (b) at 22 °C and 37 °C. All hydrogels were formed at c_{tot}=3.0 wt% and polymer/aCNC mass ratio 1/1. (c) Variation in differential modulus, K', for Gel-H5 at 22 and 37 °C.

The results shown in Fig. S13 show substantial reproducibility of the nonlinear strain-stiffening behavior of Gel-H5. Three repetitive shear experiments were performed with 20-min time interval between them, with the maximum shear stress and strain of 200 Pa to avoid gel fracture. In comparison with the first experiment, the value of *K*' reduced by 9.5 and 4.0% in experiment 2 and 3, respectively.

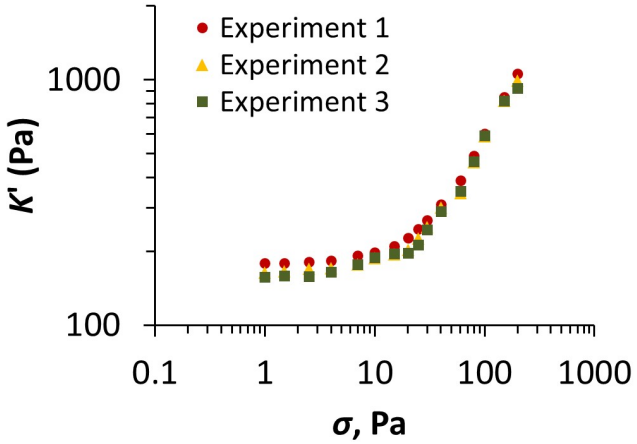

Fig. S13. Variation in the differential modulus K' with the shear stress in three repetitive experiments performed for Gel-H5 (c_{tot}=3.0 wt% and polymer/aCNC mass ratio 1/1). The relaxation time between shear experiments was 20 min.

S4. Theoretical prediction of strain stiffening of the hydrogel

The detailed description of the theoretical predictions of hydrogel's nonlinear mechanical properties is given in previous reports published by our group.[14,16] Below we provide only key equations pertinent to the results of the current work. In the hydrogels, the filaments between the cross-linking points are not freely jointed due to the covalent crosslinking of the hydrogel network. Thus, we consider the bending and stretching movements of fibers and assume that crosslinking points are not destroyed in the region of applied deformation. We consider different deformation regimes, based on the relation between γ *vs.* σ, that is, (i) the linear dependence γ *vs.* σ at $\gamma < \gamma_s$ and $\sigma < \sigma_s$; (ii) the region where fiber dissipate stress at $\gamma_s < \gamma < \gamma_c$ and $\sigma_s < \sigma < \sigma_c$; and (iii) strain-stiffening at $\gamma > \gamma_c$ and $\sigma > \sigma_c$ **(Fig. S14)**.

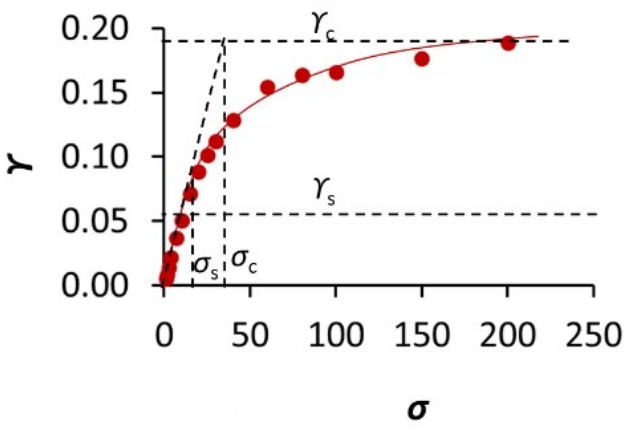

Fig. S14. Characteristics of the nonlinear shear behavior of hydrogels. Dependence of γ *vs.* σ for the hydrogels, used to determine the critical stress, σ_c, and critical strain, γ_c, as well as the linear region for stress and strain variation, σ_s and γ_s.

In first regime ($\gamma < \gamma_s$), the filaments are only weakly stretched, and the elasticity of the gel with the shear modulus given by $G \approx \nu k_b$ is determined primarily by filament bending. The response of the gel is linear $\gamma \approx \sigma/G$, with elastic energy $\nu k_b \gamma^2/2$ and the differential modulus given by[14]

$$K' = \frac{d\sigma}{d\gamma} = G \approx \nu k_b \quad at \quad \sigma < \sigma_s = G\gamma_s \tag{S12}$$

For strong shear deformation in regimes (ii) and (iii) at $\gamma > \gamma_s$, the filaments oriented mainly along the axis of maximum shear deformation and are stretched, while the filaments oriented in the compression direction are bent, and filament stretching starts at $\gamma > \gamma_s$. The fraction of stretched filaments φ_s is small for the shear strain γ above, but close to γ_s, that is, for $\gamma - \gamma_s \ll \gamma_s$ (**Fig. S9**). We consider the fraction of stretched filaments φ_s by the first term of the Taylor expansion $\varphi_s = a_\gamma(\gamma - \gamma_s) \ll 1$ in powers of $\gamma - \gamma_s$ with the expansion coefficient $a_\gamma \sim 1$. Assuming affine deformation of the stretched filaments, we estimate the elastic energy of the gel ΔE as the sum of bending and stretching contributions. [14]

The experimental dependence K'/G'_0 *vs*. σ/σ_c followed the theoretical prediction[14,16] (the solid line in Fig. 4c, main text) which was calculated as

for $\sigma_s < \sigma < 2\sigma_c - \sigma_s$ $$K' = G\sqrt{1 + \frac{6k_s a_\gamma \gamma_s}{k_b}\left(\frac{\sigma}{\sigma_c} - 1\right)} \tag{S13}$$

and

for $\sigma > 2\sigma_c - \sigma_s$ $$K' = G\frac{\sigma}{\sigma_c} \tag{S14}$$

Here $a_\gamma \sim 1$ is the expansion coefficient in $\varphi_s = a_\gamma(\gamma - \gamma_s)$, where φ_s is the fraction of stretched filaments under strain γ, and G' is the shear modulus of the hydrogel

$$K' = \nu k_b + 3\nu k_s a_\gamma(\gamma - \gamma_s) \quad \text{for } \gamma > \gamma_s \tag{S15}$$

and

$$\gamma_c = \frac{\sigma_c}{G} \qquad \text{for } \gamma > \gamma_s, \tag{S16}$$

where ν is the number density of fibers in the undeformed gel (determined from $G \approx \nu k_b$).

Fig. S15 shows the dependence of the nonlinear coefficient m and critical stress σ_c on concentration of hydrazone crosslinks in the hydrogels.

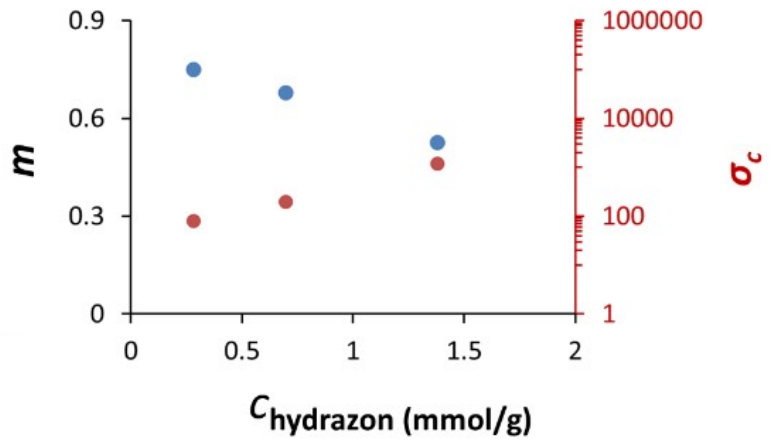

Fig. S15. Nonlinear mechanical parameters of hydrogels. Variation in the critical stress σ_c and nonlinear coefficient m on concentration of hydrazone crosslinks.

With an increasing concentration of hydrazone crosslinks the nonlinearity coefficient, m, decreased, which was caused by increasing fiber rigidity.

Figure S16a shows the variation in the hydrogel shear storage modulus, G', for physical gel based on aCNC and HBSS (PhysGel), covalent gel based on copolymer pAm-Hyd5 (CovGel), and aCNC and gels formed by both physical and covalent bonds Gel-H5.

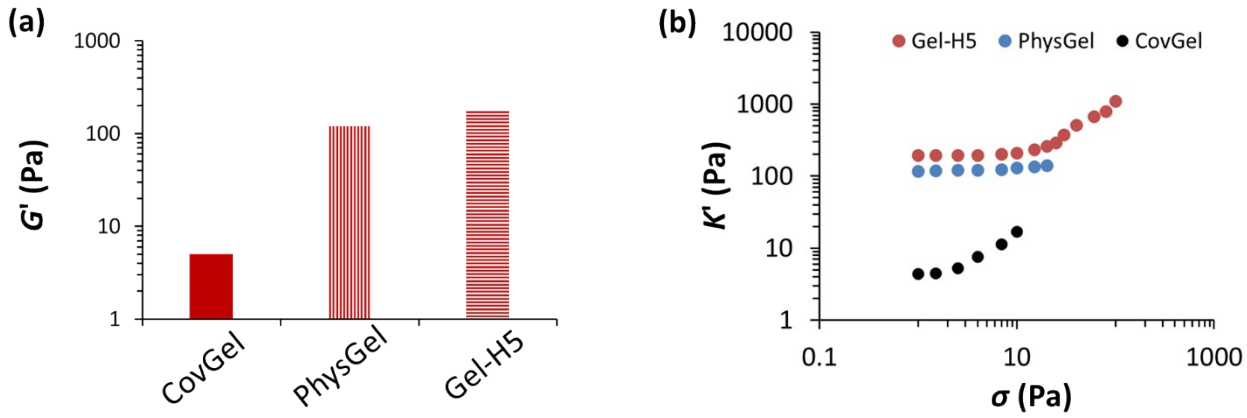

Fig. S16. Mechanical properties of the hydrogels. Variation in the storage modulus, G' (a) and G'' (b) at r.t. (22 °C) and biologically relevant temperature (37 °C). All hydrogels were formed at c_{tot}=3.0 wt% and polymer/aCNC mass ratio 1/1.

S5. Theoretical prediction of compression-induced softening of the hydrogel and reproducibility details

For compression-induced softening the theoretical prediction of the shear modulus was given by [14]

$$G^{'}(\varepsilon_z) \simeq \left(1 + \frac{12}{7}\varepsilon_z - \frac{4}{7}\varepsilon_z^2\right) G'(\varepsilon_z = 0) \quad \text{for} \quad \varepsilon_z < \varepsilon_s \qquad \text{(S17)}$$

For $\varepsilon_z > \varepsilon_s$ the filaments oriented in the direction of maximum gel stretching were completely straightened. Further filament extension was governed by their stretching stiffness, which was significantly higher than their bending stiffness ($k_s \gg k_b$) Therefore, the value of $G^{'}(\varepsilon_z)$ predicted by Eq. 17 was greater than what? and for higher degrees of gel deformation the following equation was used [14]

$$G^{'}(\varepsilon_z) \simeq \left(1 + \frac{12}{7}\varepsilon_z - \frac{4}{7}\varepsilon_z^2\right)\left[1 + \frac{3k_s a_\varepsilon}{k_b}(\varepsilon_z - \varepsilon_s)\right] G'(\varepsilon_z = 0) \quad \text{for } \varepsilon > \varepsilon_s \qquad \text{(S18)}$$

Fig. S17a shows the variation in the ratio G'/G'_0 with applied strain ε_z for Gel-H5, with different time intervals time between each the experiment (increase or decrease of ε_z with rate 0.1 μm/s). The value of G' was determined at 1% oscillatory shear strain and a frequency of 1 Hz, following 1-min equilibration at each axial strain. Compression-induced softening was observed when the time interval between the experiments was 5 or 15 min. Fig. S15b shows that in three sequential experiments conducted with 15-min relaxation time between them the variation in G'/G'_0 was reproducible, with standard deviation in the G'/G'_0 value not exceeding 7%.

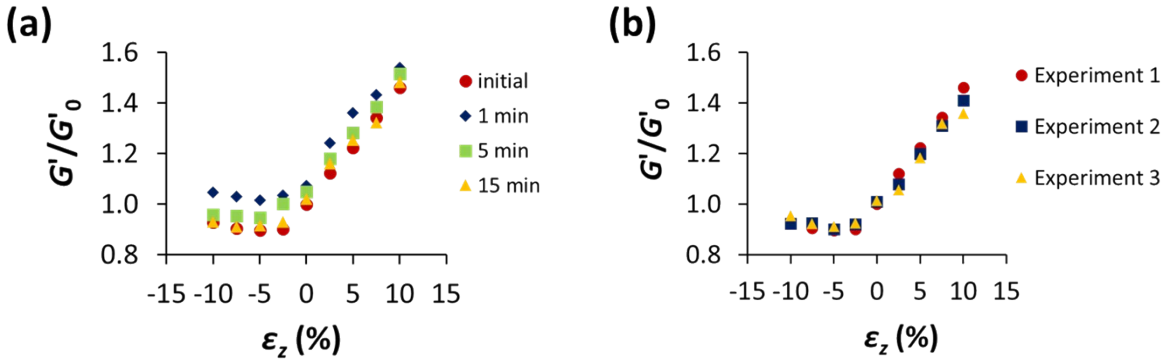

Fig. S17. Examination of reproducibility of the compression-induced softening behavior for Gel-H5. (a) Variation in G'/G'_0 versus ε_z examined at different time intervals between the experiments (an increase or decrease in ε_z). (b) Variation in G'/G'_0 with ε_z in three sequential experiments performed with 15-min relaxation time between them. “

References

[1] D. N. Crisan, O. Creese, R. Ball, J. L. Brioso, B. Martyn, J. Montenegro, F. Fernandez-Trillo, *Polym Chem* **2017**, *8*, 4576.

[2] E. A. Hoff, B. A. Abel, C. A. Tretbar, C. L. McCormick, D. L. Patton, *Polym Chem* **2017**, *8*, 4978.

[3] Y. Iwasaki, H. Maie, K. Akiyoshi, *Biomacromolecules* **2007**, *8*, 3162.

[4] X.-Y. Qi, N. O. Keyhani, Y. C. Lee, *Anal Biochem* **1988**, *175*, 139.

[5] E. Madruga, *Prog Polym Sci* **2002**, *27*, 1879.

[6] A. Kumar, R. R. Ujjwal, A. Mittal, A. Bansal, U. Ojha, *ACS Appl Mater Interfaces* **2014**, *6*, 1855.

[7] H. Li, T. Chen, B. Wu, X. Jin, J. Liu, M. Bao, *European J Org Chem* **2025**, *28*, DOI 10.1002/ejoc.202401233.

[8] X. Tian, X. Jiang, *Cellulose* **2018**, *25*, 987.

[9] J. Sirvio, U. Hyvakko, H. Liimatainen, J. Niinimaki, O. Hormi, *Carbohydr Polym* **2011**, *83*, 1293.

[10] K. H. Bouhadir, D. S. Hausman, D. J. Mooney, *Polymer (Guildf)* **1999**, *40*, 3575.

[11] M. Chau, S. E. Sriskandha, D. Pichugin, H. Thérien-Aubin, D. Nykypanchuk, G. Chauve, M. Méthot, J. Bouchard, O. Gang, E. Kumacheva, *Biomacromolecules* **2015**, *16*, 2455.

[12] D. Ciftci, A. Ubeyitogullari, R. R. Huerta, O. N. Ciftci, R. A. Flores, M. D. A. Saldaña, *J Supercrit Fluids* **2017**, *127*, 137.

[13] Y. Huang, S. M. Morozova, T. Li, S. Li, H. E. Naguib, E. Kumacheva, *Biomacromolecules* **2023**, *24*, 1173.

[14] E. Prince, S. Morozova, Z. Chen, V. Adibnia, I. Yakavets, S. Panyukov, M. Rubinstein, E. Kumacheva, *Proc. Nat. Acad. Scie* **2023**, *120*, DOI 10.1073/pnas.2220755120.

[15] Y. Huang, S. M. Morozova, T. Li, S. Li, H. E. Naguib, E. Kumacheva, *Biomacromolecules* **2023**, *24*, 1173.

[16] Y. Li, Y. Li, E. Prince, J. I. Weitz, S. Panyukov, A. Ramachandran, M. Rubinstein, E. Kumacheva, *Nat Commun* **2022**, *13*, 3264.

[17] L. Korson, W. Drost-Hansen, F. J. Millero, *J Phys Chem* **1969**, *73*, 34.